PHYSICAL REVIEW B **94**, 140409(R) (2016)

Long-range antiferromagnetic interactions in Ni-Co-Mn-Ga metamagnetic Heusler alloys: A two-step ordering studied by neutron diffraction

F. Orlandi,[1,2,*] S. Fabbrici,[3] F. Albertini,[3] P. Manuel,[1] D. D. Khalyavin,[1] and L. Righi[2]

[1]*ISIS Pulsed Neutron Facility, STFC, Rutherford Appleton Laboratory, Chilton, Didcot, Oxfordshire OX11-0QX, United Kingdom*

[2]*Dipartimento di Chimica, Università di Parma, Parco Area delle Scienze 17/A, 43124 Parma, Italy*

[3]*IMEM-CNR, Parco Area delle Scienze 37/A, 43124 Parma, Italy*

(Received 14 July 2016; revised manuscript received 8 September 2016; published 11 October 2016)

We report on the experimental observation of a long-range antiferromagnetic structure in the metamagnetic Ni-Co-Mn-Ga Heusler alloys. The accurate magnetic symmetry analysis based on experimental neutron diffraction data, exploiting the Shubnikov theory, allows the determination of the correct magnetic space group of the system. A two-step process, featuring the ordering of the Ni and Mn sublattices at different temperatures, leads to the antiferromagnetic structure in martensite. A perfect, constrained by the symmetry, antiferromagnetic ordering of the Ni sublattice in the "paramagnetic gap" is observed, followed by the ordering of the Mn sublattice at lower temperatures. The observation of such antiferromagnetic structure clarifies the current debate on the presence of antiferromagnetic interactions in the (Ni,Co)-Mn-X (X = Ga, Sn, Sb, and In) ferromagnetic shape memory alloys and yields new insights in understanding the magnetostructural properties of this relevant class of materials.

DOI: 10.1103/PhysRevB.94.140409

Intermetallic Heusler compounds are an exciting class of materials for solid state physicists and materials scientists. Due to the high number of elements which can be accommodated in the Heusler scaffold and to the flexibility of their electronic structures, novel phenomena and properties have constantly emerged in recent years, paving the way to innovative multifunctional applications in many technological sectors [1–4].

The Heusler system X_2YZ, usually crystallizing in an $L2_1$ structure, consists of four interpenetrating fcc lattices (see Fig S1 in the Supplemental Material [5]), two occupied by the X atom, generating a simple cubic lattice, and two by the Y and Z atoms forming an NaCl arrangement. In general, X and Y sites are occupied by d and f elements, whereas Z sites are occupied by a IIIA-VA group element. Quaternary Ni-Co-Mn-X (X = Ga, Sn, In. and Sb) alloys have attracted considerable interest thanks to the coexistence of magnetically ordered states and martensitic instability: the interplay between the reversible structural transformation and magnetism gives rise to a series of peculiar features, such as magnetic shape memory and superelasticity [6,7], giant caloric effects (magneto-, baro- and elastocaloric effects) [8–14], and exchange-bias effects [15,16] which make these materials promising for novel applications in the fields of sensors, actuators, and energy conversion devices.

Ni-Co-Mn-Ga alloys exhibit a martensitic transformation associated with an abrupt decrease of the magnetization crossing from the high-temperature high-magnetization austenitic phase to the low-temperature low-magnetization or eventually paramagneticlike martensite [11,12]. On further cooling below the structural transition, the occurrence of a sudden increase of magnetization, described as the Curie temperature of the martensite (T_C^{M}), is observed [11,12]. Similar magnetic behavior was also accounted for other Ni-Mn-X (X = In, Sn, and Sb) systems [7,17,18]. Despite many effects arising from the martensitic transformation [6–16], a clear account of the magnetic ground state is still missing. The gap comprised between the structural transition and T_C^{M} is generally interpreted as a paramagnetic state [11,12] and referred to as "paramagnetic gap". Nevertheless, new investigations show the presence of antiferromagnetic (AFM) interactions in this temperature region [19,20].

Structural and magnetic investigations were undertaken in order to explore the nature of the magnetic interactions at the basis of the magnetization collapse below the martensitic transformation [18–26]. Neutron polarization analysis experiments [19] performed on $Ni_{50}Mn_{37}Sn_{13}$ clearly indicate the presence of AFM correlations in the paramagnetic gap confirmed also by ferromagnetic resonance measurements [20]. On the other hand, Mössbauer experiments conducted on iron-substituted $Ni_{50}Mn_{34.8}In_{15.2}$ [21] and $Ni_{50}Mn_{37}Sn_{13}$ [22] indicate paramagnetism of the Mn sites in the gap and complex magnetic interactions below T_C^{M}. Another indication of the coexistence of ferro and antiferro interactions in these types of systems is the experimental observation of exchange-bias effects in magnetically ordered martensite [4,15,16,18]. In the complex scenario of the Heusler alloys, including, for example, inverse Mn_2PtGa or Mn_3Ga ordered tetragonal systems [4], the chemical control of the sublattice sites determines the progressive enhancement of exchange-bias effects [4,15,16,18]. The vast literature questioning the nature of the antiferromagnetic interactions in Heusler materials proposed few possible ferrimagnetic models and such ordered distributions of spins were investigated by theoretical studies without considering a possible pure antiferromagnetic condition [4,27–29].

In the present work, we report on the observation of a long-range antiferromagnetic ordered state in a Ni-Co-Mn-Ga Heusler tetragonal martensite. The accurate magnetic symmetry analysis, exploiting the use of the Shubnikov space groups [30], allows us to provide results related to the symmetry of the martensitic magnetic state and to the mutual interplay between the different magnetic sublattices. The structural insights hereafter discussed open up another viewpoint for the comprehension of the complex exchange topology ruling the "Heusler magnetism".

*Corresponding author: fabio.orlandi@stfc.ac.uk

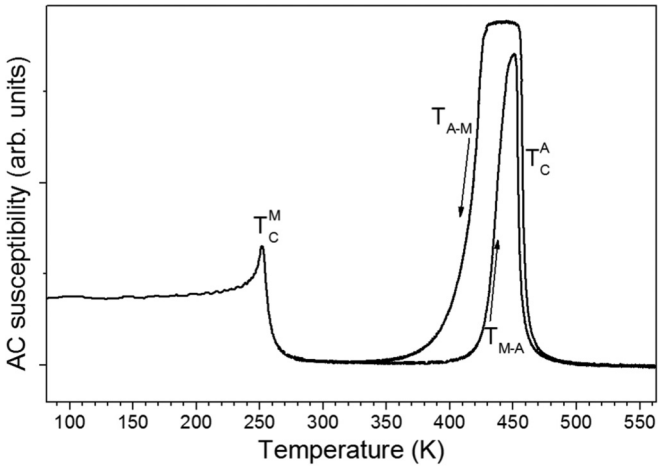

FIG. 1. Temperature evolution of ac susceptibility of the $Ni_{41}Co_9Mn_{32}Ga_{18}$ compound. The transition temperatures are underlined in the plot: T_C^M and T_C^A indicate the Curie temperatures of the martensitic and austenitic phases, respectively, whereas $T_{M\text{-}A}$ and $T_{A\text{-}M}$ indicate the structural transformation on heating and cooling.

The Co-based sample investigated in the present work has nominal composition $Ni_{41}Co_9Mn_{32}Ga_{18}$, and an exhaustive characterization of the magnetic and structural properties appeared in earlier publications [11,12]. Figure 1 illustrates the thermomagnetic analysis (TMA) highlighting the critical temperatures of the system. From these measurements the compound shows the transition from a ferromagnetic austenite to a paramagnetic or antiferromagneticlike martensite at $T_{A\text{-}M}$. By further cooling a sudden increase of the ac susceptibility is detected around 250 K; as previously discussed, this transition is generally associated, in literature, with the Curie temperature of the martensitic phase (T_C^M) [11,12].

The crystallographic study of $Ni_{41}Co_9Mn_{32}Ga_{18}$ was performed through time of flight neutron diffraction data obtained at the ISIS facility (UK) on the WISH diffractometer [31] in a wide range of temperatures between 150 and 573 K; each measurement has been fitted through Rietveld refinement by using the JANA2006 software [32] on the high-resolution backscattering bank with $2\theta = 152^\circ$.

Above 450 K the system consists of a paramagnetic austenite, described (Fig. 2, top) by the ordered $L2_1$ structure with paramagnetic space group $Fm\text{-}3m1'$. The refined occupancy factors are in good agreement with the nominal composition and the energy-dispersive x-ray measurements ($Ni_{41.85}Co_{9.14}Mn_{32.05}Ga_{16.96}$). As expected, Co is located at the Ni sites, while the exceeding Mn is located in the Ga sublattice.

On cooling below $T_{A\text{-}M}$ the compound shows a complete martensitic transformation to a nonmodulated tetragonal structure [12]. The refinement with an $I4/mmm1'$ structure, derived from the austenitic phase, shows good agreement regarding the main reflections, but as highlighted in Fig. 2 some diffraction peaks remain unindexed: two of such reflections show a strong, nonlinear, thermal evolution of the integrated intensity [see as an example in Fig. 3 the (100) reflection] and form factor dependence, indicating that they are due to magnetic scattering. It is important to note that the extra magnetic peaks

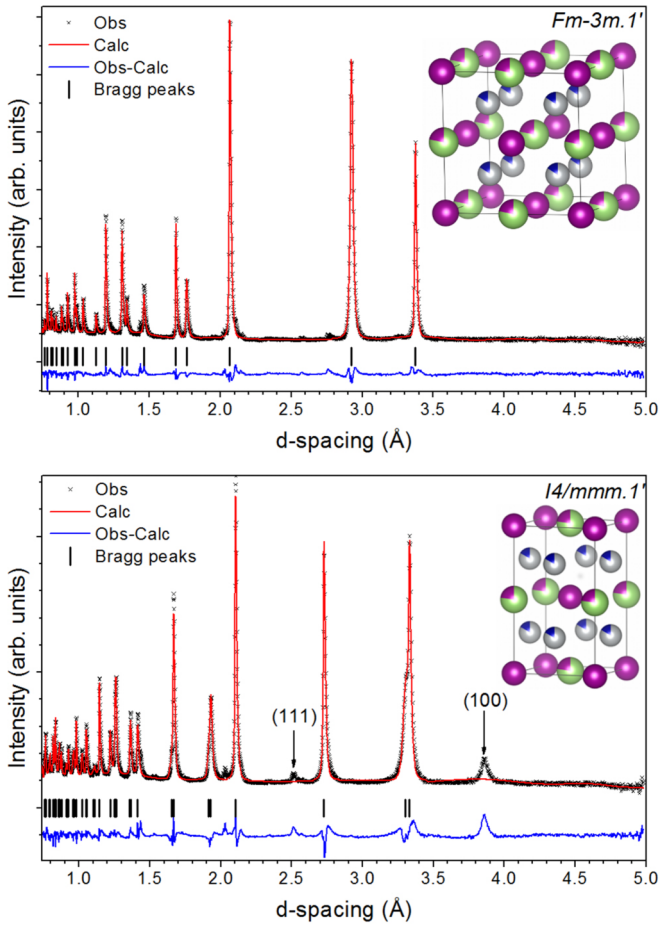

FIG. 2. Top: Rietveld plot of the austenitic phase at 573 K in the $Fm\text{-}3m1'$ space group. Bottom: Rietveld plot of the martensitic phase at 285 K where only the nuclear contribution is taken into account. In both panels observed (×, black), calculated (red line), and difference (blue line) patterns are reported. The tick marks indicate the Bragg reflection position, while in the bottom panel the black arrows indicate the unindexed reflections. The insets provide a sketch of the structures: purple (dark gray) spheres represent the manganese atoms, and green (big, light gray) and silver (small, light gray) spheres represent the gallium and nickel sites, respectively. The agreement factors are $R_p = 3.62\%$, $R_{wp} = 4.83\%$ (top) and $R_p = 5.33\%$, $R_{wp} = 6.65\%$ (bottom). The weak unindexed reflections observed at 2.0 and 2.3 Å are due to highly textured aluminum coming from the sample environment.

are clearly detectable just below $T_{M\text{-}A}$, and that the full width at half maximum of these reflections is comparable with the nuclear peaks, indicating a long-range magnetic ordering in the widely recognized "paramagnetic gap." A further peak is found at high d spacing: its position corresponds to the (001) reflection of martensite, yet it is extremely weak and much broader than any other peak of the pattern. Furthermore, its temperature dependence suggests a different nature with respect to the other additional peaks (see Fig. 3): systematic defects, subtle structural distortions, or magnetic contributions could be the origin of such reflections, yet further data is required to better clarify its nature.

In principle, accounting for this extra reflection as due to nuclear distortions removes the I-centering symmetry

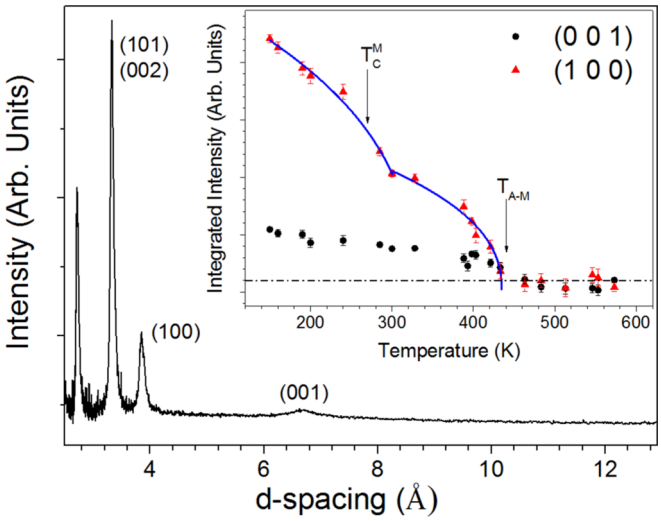

FIG. 3. Diffraction pattern collected at 150 K in the forward scattering bank of the WISH instrument ($2\theta = 27°$) showing the weak and broad (001) reflection in comparison with the (101) and (002) nuclear reflections and the magnetic (100) reflection. Inset: Integrated intensity of the (001) and (100) reflections in the tetragonal unit cell versus temperature; the blue line is a guide for the eyes.

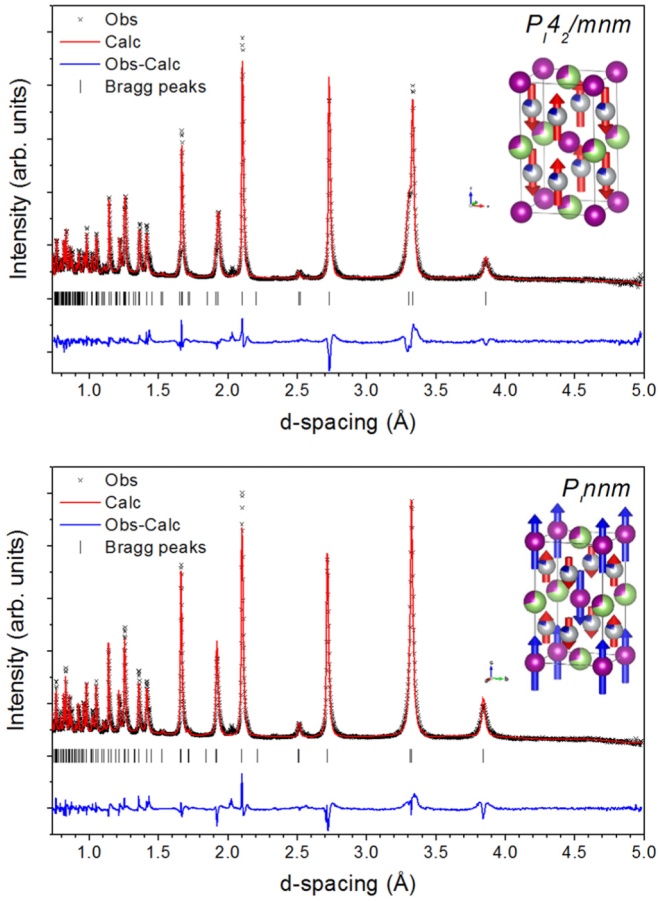

FIG. 4. Top: Rietveld plot of the magnetic martensitic phase in the paramagnetic gap collected at 285 K: the structure is described in the P_I4_2/mnm magnetic space group, the agreement factors being $R_p = 3.62\%$, $R_{wp} = 4.83\%$. Bottom: Rietveld plot of the magnetic martensite collected at 150 K below T_C^M in the P_Inm magnetic space group, agreement factors $R_p = 5.40\%$, $R_{wp} = 6.64\%$. Both panels display observed (×, black), calculated (red line), and difference (blue line) patterns. The tick marks indicate the Bragg reflection positions. The insets provide a sketch of the structures, with arrows indicating the directions of the ordered magnetic moments.

operator; nonetheless, the refinements performed lowering the symmetry to primitive space groups systematically converged to solutions coherent with *I*-centered structure. The structural distortion at the basis of the lattice symmetry breaking has therefore a limited impact on the average crystalline martensitic phase, thus a comprehensive refinement of the atomic positions and occupancies in the primitive cell does not return valuable additional information. For these reasons we will focus the structural analysis on the average basic structure (with $I4/mmm1'$ symmetry) disregarding the slight structural deviation, and discuss later in detail the effect of the *I*-centering symmetry breaking on the interpretation of the magnetic structure at low temperatures.

A review of existing literature provides two magnetic structural models for the tetragonal Heusler alloys [4,27–29,33–35]. The first one comprises a ferromagnetic arrangement of all the sublattices in the structure. The second model, acknowledging two different sublattices antiferromagnetically coupled, can be described as the ferromagnetic spin orientation of the fully occupied Mn sublattice of the Na-Cl-like scaffold, while the extra-Mn atoms located in the sublattice formed by III-VA atomic species show an inverse spin arrangement. Both these structures derive from the $I4/mmm1'$ space group as the parent symmetry and are described in the $I4/mm'm'$ magnetic space group for an axial anisotropy or in the $Im'm'm$ for an in-plane one. Both models correspond to a $\kappa = (000)$ propagation vector, but are clearly not in agreement with the observed diffraction pattern, since the magnetic peaks highlighted in Fig. 2 unambiguously violate the *I*-centering systematic absences, corresponding to the $\kappa = (111)$ propagation vector.

The symmetry analysis of the magnetic structure was performed with the help of the ISODISTORT software [36]: a detailed description of the symmetry and structural analysis is reported in the Supplemental Material [5]. The best agreement between calculated and observed data, in terms of reliability factors [5], is obtained for the P_I4_2/mnm symmetry. In this magnetic space group the site symmetry of the Mn and Ga sublattices ($4'/mm'm$) forbids moment ordering, whereas the site symmetry of Ni/Co site ($-4m'2'$) allows an ordered alignment of the spins. The resulting magnetic structure is composed of localized moments at the Ni/Co sites, organized in ferromagnetic rows along the ***c*** axis coupled antiferromagnetically with the four neighboring ones, as shown in the top inset of Fig. 4. The Rietveld refinement based on this magnetic model converges with good agreement factors, with an ordered moment at the Ni/Co sites of $0.95(2)\mu_B$ at 285 K, close to the theoretical value expected in the case of almost localized moment. It is important to note that this magnetic model is in agreement with all the previous experimental studies on the magnetic interactions in the so-called paramagnetic gap, which report on the one hand the presence of AFM interactions [19,20] and

on the other hand, the observed paramagnetic condition of Mn atoms [11,21,22]. It is worth stressing that magnetic diffuse scattering, indicating the presence of short-range magnetic ordering, has already been observed in the Ni-Mn-Sn systems just below the martensitic transition [19]. Considering the actual results, the observed diffuse scattering can be interpreted in terms of a short-range antiferromagnetic ordering of the Ni sublattice.

By crossing down T_C^M, experimental data reveal a sudden increase of the magnetic intensity related to the AFM structure without the rise of new extra reflections. Since it has been previously verified that the crossing of T_C^M does not affect the structure [12], it is reasonable to suppose that the additional magnetic intensity, observed below T_C^M, is due to an ordering of the Mn sublattices. This additional magnetic ordering necessarily requires a symmetry reduction, since in the P_I4_2/mnm space group the site symmetry of Mn sublattice does not allow a dipole magnetic moment. Therefore the order 2 subgroups of P_I4_2/mnm were tested and the best agreement between observed and calculated data was obtained for the P_Innm magnetic space group, which is also the only subgroup that allows an ordered moment on the Mn site [5]. The obtained magnetic ordering of the Mn sublattice is constituted by ferromagnetic ***ac*** planes coupled antiferromagnetically along the ***b*** direction. The refined magnetic moment for Mn at 150 K is $1.64(10)\mu_B$; the magnetic moment of the Ni/Co site at the same temperature is $0.97(5)\mu_B$, very close to the RT value [5]. It should be pointed out that the localized Mn moment is lower than the value usually assumed in the theoretical models based on ferromagnetic intrasublattices ordering. The values obtained in the present study, however, are close to those derived for the parent NiMn alloy with the well-established antiferromagnetic structure [20].

The experimental evidence, provided here, unambiguously determines the presence of an AFM arrangement in all the sublattices of the martensitic phase, imposed by the magnetic symmetry. This is different from the previously proposed models [4,27–29]. It is, however, important to point out that the P_Immm space group does not allow any ferromagnetic component, in contrast with the rise of susceptibility below T_C^M observed by TMA in Fig. 1. In this context a net magnetization contribution is expected to arise from the off-stoichiometry: although the Mn/Ga mixed site shares the same point symmetry as the Mn one, leading to AFM interactions within the sublattice, the uncompensated exchange interactions due to partial Mn occupancy might be responsible for the resulting magnetization [37,38].

As a final test of the actual model we have lowered the symmetry to reflect the subtle breaking of the body centered lattice requested by the presence of the weak (001) reflection. This reflection has linear temperature dependence (Fig. 2) and exists only in the martensitic phase (Fig. 3), which strongly testifies that the associated distortions should not be ascribed to atomic ordering of Mn and Ga in the shared site, but might be induced through the magnetoelastic coupling allowed in both P_I4_2/mnm and P_Innm space groups. If we consider this reflection as evidence of the *I* centering breaking, this allows the further reduction of the magnetic symmetry to $P4'/mm'm$ and $Pm'm'm$, respectively, explaining the observed ferromagnetic moment. Above T_C^M, in the so-called paramagnetic gap, the magnetic symmetry constraint for the Ni/Co sublattice ($2m'm'$) gives rise to the same AFM alignment observed in the P_I4_2/mnm magnetic space group; the Mn and Mn/Ga sites are now split into two couples of inequivalent positions, yet their site symmetries ($4'/mm'm$) are unaffected by the removal of the *I*-centering operator, preventing, as in the previous interpretation, the magnetic ordering of the Mn atoms. As a result, the structural refinement performed on the primitive group provides the same reciprocal spin orientation as the *I*-centered solution. Below T_C^M the primitive space group is now $Pm'm'm$; the lower symmetry enables two independent positions for all three sublattices [5], nevertheless the refinement confirms the antiparallel alignment of all the sublattices as found in the *I*-centered model. In detail, the Ni/Co sites converge towards a perfect AFM alignment, while refinement on the Mn site suggests the presence of a small uncompensated moment, which leads to a ferrimagnetic net contribution in accordance with the magnetic susceptibility measurement. To test the solidity of our solution we performed further testing by introducing some arbitrary constraints on the magnetic alignment other than the antiparallel one: the refinement was always found either to diverge or to collapse back to the *I*-centered solution.

In conclusion, we have shown a clear indication of antiferromagnetic ordering in the Ni-Co-Mn-Ga Heusler alloy, providing a comprehensive symmetry analysis of the magnetic structure in the martensitic phase and the temperature evolution of the magnetic interactions within the various sublattices. In particular, the magnetic structure of martensite has been consistently described as a two-step ordering process involving the Ni/Co sites and the Mn/Ga ones. The observation of magnetic reflections at ~285 K is direct evidence of magnetic ordering in the paramagnetic gap. In this temperature region, we observed an antiferromagnetic ordering of the Ni/Co lattice and introduced a magnetic structure model, hitherto not considered by theoretical studies. The Mn site orders antiferromagnetically below T_C^M, but the resolution of the neutron diffraction experiment does not allow us to uniquely evaluate the extent of the ferromagnetic component observed below this temperature in the TMA measurement. The establishment of such detail requires further structural studies, combining neutron and high-resolution x-ray synchrotron diffraction measurements on compositions with different degrees of nonstoichiometry. Nonetheless, the present results are fundamental in understanding the physical properties of these materials and our present study should spur further theoretical work, starting from the observed paramagnetic gap and exchange bias measured at low temperature [11,15,16,39]. The latter is generally explained as the clustering of a ferromagnetic region within a ferrimagnetic matrix which act as a pinning environment: Nayak *et al.* [4] point out that in order to obtain high values of the exchange-bias field the ferrimagnetic matrix must be as close as possible to the antiferromagnetic state. In the present case, the direct observation of a symmetry constrained antiferromagnetic matrix opens up new prospects on the exchange-bias effect in metamagnetic Heusler alloys.

The authors acknowledge the Science and Technology Facilities Council for providing neutron beam time.

[1] T. Graf, C. Felser, and S. P. Parkin, Prog. Solid State Chem. **39**, 1 (2011).

[2] *Heusler Alloys*, edited by C. Felser and A. Hirohata, Springer Series in Materials Science Vol. 222 (Springer, Switzerland, 2016).

[3] S. Chadov, X. L. Qi, J. Kubler, G. H. Fecher, C. Felser, and S. C. Zhang, Nat. Mater. **9**, 541 (2010).

[4] A. K. Nayak, M. Nicklas, S. Chadov, P. Khuntia, C. Shekhar, A. Kalache, M. Baenitz, Y. Skourski, V. K. Guduru, A. Puri, U. Zeitler, J. M. D. Coey, and C. Felser, Nat. Mater. **14**, 679 (2015).

[5] See Supplemental Material at http://link.aps.org/supplemental/10.1103/PhysRevB.94.140409 for details of the crystallographic analysis, crystal structure information, table with atoms coordinates, bond lengths and cell parameter temperature evolution, magnetic symmetry analysis result, and mcif files.

[6] H. E. Karaca, I. Karaman, B. Basaran, Y. Ren, Y. I. Chumlyakov, and H. J. Maier, Adv. Funct. Mater. **19**, 983 (2009).

[7] R. Kainuma, Y. Imano, W. Ito, Y. Sutou, H. Morito, H. Okamato, S. Kitakami, O. Oikawa, A. Fujita, T. Kanomata, and K. Ishida. Nature (London) **439**, 957 (2006).

[8] J. Liu, T. Gottschall, K. P. Skokov, J. D. Moore, and O. Gutfleisch, Nat. Mater. **11**, 620 (2012).

[9] T. Krenke, E. Duman, M. Acet, E. F. Wassermann, X. Moya, L. Mañosa, and A. Planes, Nat. Mater. **4**, 450 (2005).

[10] A. Planes, L. Manosa, and M. Acet, J. Phys.: Condens. Matter **21**, 233201 (2009), and references within.

[11] S. Fabbrici, J. Kamarad, Z. Arnold, F. Casoli, A. Paoluzi, F. Bolzoni, R. Cabassi, M. Solzi, G. Porcari, C. Pernechele, and F. Albertini, Acta Mater. **59**, 412 (2011).

[12] S. Fabbrici, F. Albertini, A. Paoluzi, F. Bolzoni, R. Cabassi, M. Solzi, L. Righi, and G. Calestani, Appl. Phys. Lett. **95**, 022508 (2009).

[13] L. Mañosa, D. González-Alonso, A. Planes, E. Bonnot, M. Barrio, J. L. Tamarit, S. Aksoy, and M. Acet, Nat. Mater. **9**, 478 (2010).

[14] R. Millán-Solsona, E. Stern-Taulats, E. Vives, A. Planes, J. Sharma, A. K. Nayak, K. G. Suresh, and L. Mañosa, Appl. Phys. Lett. **105**, 241901 (2014).

[15] M. Khan, I. Dubenko, S. Stadler, and N. Ali, J. Phys.: Condens. Matter **20**, 235204 (2008).

[16] M. Khan, I. Dubenko, S. Stadler, and N. Ali, Appl. Phys. Lett. **102**, 232406 (2013).

[17] A. Çakır, L. Righi, F. Albertini, M. Acet, and M. Farle, Acta Mater. **99**, 140 (2015).

[18] A. K. Pathak, M. Khan, B. R. Gautam, S. Stadler, I. Dubenko, and N. Ali, J. Magn. Magn. Mater. **321**, 963 (2009).

[19] S. Aksoy, M. Acet, P. P. Deen, L. Manosa, and A. Planes, Phys. Rev. B **79**, 212401 (2009).

[20] M. Acet and E. F. Wassermann, Adv. Eng. Mater. **14**, 523 (2012).

[21] V. V. Khovaylo, T. Kanomata, T. Tanaka, M. Nakashima, Y. Amako, R. Kainuma, R. Y. Umetsu, H. Morito, and H. Miki, Phys. Rev. B **80**, 144409 (2009).

[22] R. Y. Umetsu, R. Kainuma, Y. Amako, Y. Taniguchi, T. Kanomata, K. Fukushima, A. Fujita, K. Oikawa, and K. Ishida, Appl. Phys. Lett. **93**, 042509 (2008).

[23] S. Yuan, P. L. Kuhns, A. P. Reyes, J. S. Brooks, M. J. R. Hoch, V. Srivastava, R. D. James, S. El-Khatib, and C. Leighton. Phys. Rev. B **91**, 214421 (2015).

[24] L. Wollmann, S. Chadov, J. Kübler, and C. Felser, Phys. Rev. B **92**, 064417 (2015).

[25] S. Khmelevskyi, A. V. Ruban, and P. Mohn. Phys. Rev. B **93**, 184404 (2016).

[26] A. Çakır, M. Acet, and M. Farle, Phys. Rev. B **93**, 094411 (2016).

[27] J. Kubler, A. R. Williams, and C. B. Sommers, Phys. Rev. B **28**, 1745 (1983).

[28] V. Sokolovskiy, A. Grunebohm, V. Buchelnikov, and P. Entel, Entropy **16**, 4992 (2014).

[29] K. R. Priolkar, P. A. Bhobe, D. N. Lobo, S. W. D'Souza, S. R. Barman, A. Chakrabarti, and S. Emura, Phys. Rev. B **87**, 144412 (2013).

[30] W. Opechowski, *Crystallographic and Metacrystallographic Groups* (North-Holland, Amsterdam, 1986); A. V. Shubnikov and N. V. Belov, *Colored Symmetry* (Pergamon, New York, 1964); W. Opechowski and R. Guccione, in *Magnetism*, edited by G. T. Rado and H. Suhl (Academic, New York, 1965), Chap. 3, Vol. 2A.

[31] L.C. Chapon, P. Manuel, P. G. Radaelli, C. Benson, L. Perott, S. Ansell, N. J. Rhodes, D. Raspino, D. Duxbury, E. Spill, and J. Norris, Neutron News **22**, 22 (2011).

[32] V. Petricek, M. Dusek, and L. Palatinus, Z. Kristallogr. - Cryst. Mater. **229**, 345 (2014).

[33] P. J. Brown, A. P. Gandy, K. Ishida, R. Kainuma, T. Kanomata, K.-U. Neumann, K. Oikawa, B. Ouladdiaf, and K. R. A. Ziebeck, J. Phys.: Condens. Matter **18**, 2249 (2006).

[34] A. Pramanick, X. P. Wang, K. An, A. D. Stoica, J. Yi, Z. Gai, C. Hoffmann, and X.-L. Wang, Phys. Rev. B **85**, 144412 (2012).

[35] C. V. Stager and C. C. M. Campbell, Can. J. Phys. **56**, 674 (1978).

[36] B. J. Campbell, H. T. Stokes, D. E. Tanner, and D. M. Hatch, J. Appl. Cryst. **39**, 607 (2006).

[37] L. Néel, Compes Rendus Acad. Sci. **252**, 4075 (1961) [translated in *Selected Works of Louis Néel*, edited by N. Kurti (Gordon and Breach, New York, 1988)].

[38] L. Néel, Compes Rendus Acad. Sci. **253**, 203 (1961) [translated in *Selected Works of Louis Néel*, edited by N. Kurti (Gordon and Breach, New York, 1988)].

[39] B. Wang and Y. Liu, Metals **3**, 69 (2013).